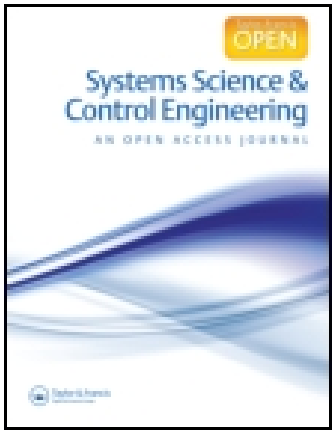

Systems Science & Control Engineering: An Open Access Journal
Publication details, including instructions for authors and subscription information: http://www.tandfonline.com/loi/tssc20

Dynamically dual vibration absorbers: a bond graph approach to vibration control

Peter Gawthrop[a], S.A. Neild[b] & D.J. Wagg[c]

[a] Systems Biology Laboratory, Melbourne School of Engineering, University of Melbourne, Victoria 3010, Australia

[b] Department of Mechanical Engineering, Queens Building, University of Bristol, Bristol BS8 1TR., UK

[c] Department of Mechanical Engineering, Sir Frederick Mappin Building, University of Sheffield, Mappin Street Sheffield S1 3JD, UK

Accepted author version posted online: 01 Dec 2014.Published online: 14 Jan 2015.

To cite this article: Peter Gawthrop, S.A. Neild & D.J. Wagg (2015) Dynamically dual vibration absorbers: a bond graph approach to vibration control, Systems Science & Control Engineering: An Open Access Journal, 3:1, 113-128, DOI: 10.1080/21642583.2014.991458

To link to this article: http://dx.doi.org/10.1080/21642583.2014.991458

Systems Science & Control Engineering: An Open Access Journal, 2015
Vol. 3, 113–128, http://dx.doi.org/10.1080/21642583.2014.991458

Dynamically dual vibration absorbers: a bond graph approach to vibration control

Peter Gawthrop[a]*, S.A. Neild[b] and D.J. Wagg[c]

[a]*Systems Biology Laboratory, Melbourne School of Engineering, University of Melbourne, Victoria 3010, Australia;* [b]*Department of Mechanical Engineering, Queens Building, University of Bristol, Bristol BS8 1TR., UK;* [c]*Department of Mechanical Engineering, Sir Frederick Mappin Building, University of Sheffield, Mappin Street Sheffield S1 3JD, UK*

(*Received 28 August 2014; accepted 20 November 2014*)

This paper investigates the use of an actuator and sensor pair coupled via a control system to damp out oscillations in resonant mechanical systems. Specifically the designs emulate passive control strategies, resulting in controller dynamics that resemble a physical system. Here, the use of the novel dynamically dual approach is proposed to design the vibration absorbers to be implemented as the controller dynamics; this gives rise to the dynamically dual vibration absorber (DDVA). It is shown that the method is a natural generalisation of the classical single-degree of freedom mass–spring–damper vibration absorber and also of the popular acceleration feedback controller. This generalisation is applicable to the vibration control of arbitrarily complex resonant dynamical systems. It is further shown that the DDVA approach is analogous to the hybrid numerical-experimental testing technique known as substructuring. This analogy enables methods and results, such as robustness to sensor/actuator dynamics, to be applied to dynamically dual vibration absorbers. Illustrative experiments using both a hinged rigid beam and a flexible cantilever beam are presented.

Keywords: vibration absorber; bond graph; acceleration feedback control; dynamic dual

1. Introduction

The use of a secondary resonant mechanical systems to damp out oscillations in a resonant mechanical system by absorbing and dissipating energy has a long history and early work is summarised in the classical textbook by Den Hartog (1985). An alternative method for damping unwanted oscillations is to use some form of active vibration control. To achieve this some type of actuator and sensor system needs to be used. For example, vibrations can be damped from a mechanical system using a piezo-electric transducer and an associated electrical circuit (Hagood & von Flotow, 1991). This can have considerable advantages, although, as discussed by Moheimani & Behrens (2004) multi-modal resonant structures require sophisticated circuit synthesis.

The adjective 'passive' applied to 'system' has two different but related meanings: a physical system not containing a power source and a mathematical expression imposing the corresponding property on the input and output variables of a set of equations (Hogan, 1985; Sharon, Hogan, & Hardt, 1991; Slotine & Li, 1991). In general, this means that passive mechanical (or electrical) vibration absorbers can be replaced by a computer and associated sensor-actuator pairs which emulate the physical passivity in the equivalent mathematical sense. The algorithm implemented in the computer does not have to represent a physical system and can be designed using conventional control-theoretic methods (Balas, 1978; Fleming & Moheimani, 2005; Hong & Bernstein, 1998; Hogsberg & Krenk, 2006; Moheimani & Fleming, 2006), optimisation (Krenk & Hogsberg, 2009) or via system inversion (Ali & Padhi, 2009).

However, it can be argued that there are advantages in implementing *physical* systems within the digital computer (Gawthrop, 1995; Gawthrop, Bhikkaji, & Moheimani, 2010; Hogan, 1985; Lozano, Brogliato, Egelund, & Maschke, 2000; Ortega, Loria, Nicklasson, & Sira-Ramirez, 1998; Ortega, van der Schaft, Mareels, & Maschke, 2001; Sharon et al., 1991; Slotine & Li, 1991); this is the approach explored in this paper. In particular, the well-known relationship between dissipativity, passivity and physical systems (Lozano et al., 2000; Ortega et al., 1998, 2001; Willems, 1972) is exploited. Such energy based concepts rely on the properties of physical connections. In particular, the concept of *collocation* is a key system property in the context of active vibration control (Gawthrop et al., 2010; Preumont, 2002).

Replacing a mechanical vibration absorber by a digital computer is analogous to the well-known hybrid numerical-experimental testing technique where the structure under consideration is split into an experimental test piece (or *physical substructure*) and a numerical model

*Corresponding author. Email: peter.gawthrop@unimelb.edu.au

describing the remainder of the structure (or *numerical substructure*). Although the two coupled passive subsystems resulting from this process are stable (Anderson & Vongpanitlerd, 2006; Desoer & Vidyasagar, 1975; Lozano et al., 2000; Ortega, Praly, & Landau, 1985; Ortega et al., 2001), this stability can be destroyed by the digital implementation of the numerical substructure and the corresponding actuator and sensor dynamics that couple the substructures (Gawthrop, Wallace, Neild, & Wagg, 2007). Fortunately, this problem of coupling the numerical and experimental substructures using real-time digital implementation has been solved and a suite of techniques for robust *numerical-experimental substructuring* is now available (Blakeborough, Williams, Darby, & Williams, 2001; Gawthrop, Wallace, & Wagg, 2005; Wagg, Neild, & Gawthrop, 2008). Furthermore, the substructuring approach is particularly suitable for the type of resonant systems that are the focus of this paper (Gawthrop et al., 2007).

As discussed by Gawthrop et al. (2005), the bond-graph approach (Borutzky, 2011; Gawthrop & Bevan, 2007; Gawthrop & Smith, 1996; Karnopp, Margolis, & Rosenberg, 2012; Mukherjee, Karmaker, & Samantaray, 2006) gives a natural and convenient formulation of substructuring and control (Gawthrop, 2004; Gawthrop et al., 2005; Vink, Ballance, & Gawthrop, 2006) and the concept of actuator/sensor collocation has a clear bond graph interpretation. For these reasons, the bond-graph approach is adopted in this paper.

As discussed by Den Hartog (1985), choosing the structure of a vibration absorber for a single degree of freedom system is straightforward. However, choosing the structure for multi-degree of freedom systems such as those arising from modal decomposition is considerably more involved (Moheimani & Behrens, 2004). This complexity motivates the novel approach of this paper based on the concept of of a *dynamically dual*[1] system.

As discussed in more detail in Section 3, a dynamically dual mechanical system is obtained by interchanging the rôles of velocity and force. This concept of duality has been used for analysis of dynamical systems (Cellier, 1991; Karnopp, 1966; Samanta & Mukherjee, 1985, 1990; Shearer, Murphy, & Richardson, 1971), and this paper uses the concept to design *dynamically dual vibration absorbers* (DDVA).

Although the DDVA method originated an extension of the physically based design of Den Hartog (1985), it will be shown that the method also includes the well-established *acceleration feedback* approach (Preumont, 2002).

In summary, placing both the traditional Den Hartog mechanical vibration absorber and acceleration feedback into the wider context of the DDVA of this paper has two advantages: the method immediately extends to multi degree of freedom systems and the implementation and theoretical results (including robustness to sensor/actuator dynamics) from substructuring can be directly applied.

Section 2 reviews the substructuring approach to provide a framework for the paper. Section 3 gives the foundations of the DDVA approach; Section 3.2 focuses on the Den Hartog (1985) absorber version and Section 3.3 focuses on the acceleration feedback controller (Preumont, 2002). Section 4 discusses a number of multi-mode examples. Section 5 gives illustrative experimental results; Sections 5.1 and 5.2 experimentally verify the approach when applied to a rigid beam with an flexible joint and a flexible cantilever beam, respectively. Section 6 concludes the paper.

2. The substructuring formulation

Substructuring is a novel dynamic testing technique that allows the experimental testing of a component within the context of a larger system. This is achieved through the coupling of the physical component with a controller that numerically simulates the dynamics of the remainder of the system. Note that as the controller dynamics are designed to simulate part of a real system, the dynamics are physically realisable.

Figure 1 summarises the basic substructuring formulation Gawthrop et al. (2005) and Gawthrop, Wagg, & Neild (2009). For simplicity, Figure 1 will be assumed to represent a system with scalar quantities, although this can readily be extended to vectors. The three key parts are shown in Figure 1:

(1) **Phy** representing the physical component, with transfer function $p(s)$, to be controlled,
(2) **Num** representing the controller, with physically realisable dynamics, which is implemented numerically and has a transfer function $n(s)$,
(3) **Se**:$\mathbf{F_0}$ representing a disturbing external force, F_0,

where s is the Laplace domain independent variable. Firstly the velocity feedback case is shown, Figure 1(a) as a bond graph[2] and in Figure 1(b) as a block diagram. Here, the physical component **Phy** has a force input, $F_0 - F$, and a measured velocity output, v. In addition, the parameters in the physical system are represented by a vector, θ_p, Similarly, θ_n, represents the vector of parameters in the numerical system.

An advantage of the bond graph representation is that it emphasises the fact that the physical system **Phy** and the controller **Num** are connected by *power bonds* and thus the control system is collocated – meaning that the actuator and sensor are located at the same point. In Figure 1(a) the parts are joined by a common flow (velocity) junction denoted as **1**. The bond graph also indicates causality and **Phy** and **Num** are represented by the positive real transfer functions $p(s, \theta_p)$ and $n(s, \theta_n)$, respectively. The transfer

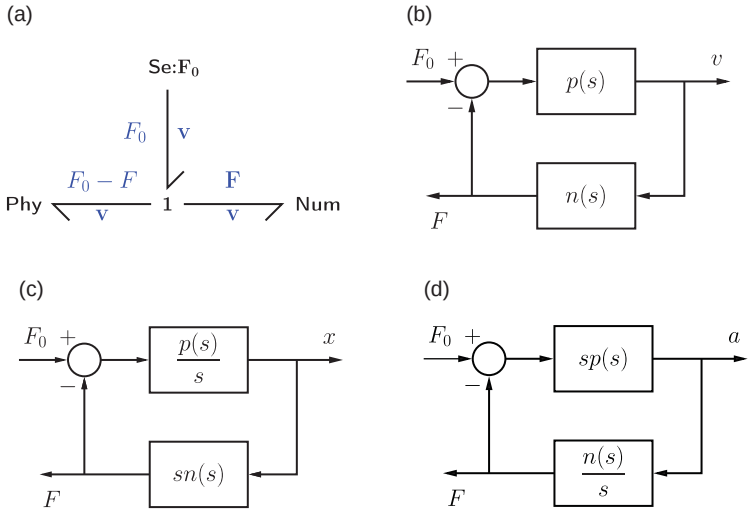

Figure 1. The substructuring formulation. The mathematically equivalent formulations (b)–(d) allow for a choice of sensors. (a) Bond graph, (b) block-diagram: velocity formulation, (c) block-diagram: displacement formulation and (d) block-diagram: acceleration formulation.

functions are related by the following relationships:

$$v = p(s, \theta_p)(F_0 - F), \tag{1}$$

$$F = n(s, \theta_n)v. \tag{2}$$

Although it is natural to work in terms of velocity v rather than displacement x, Figure 1(b) can be easily rewritten in terms of displacement as Figure 1(c) where $\mathrm{d}x/\mathrm{d}t = v$ or in terms of acceleration as Figure 1(d) where $a = \mathrm{d}v/\mathrm{d}t$. The choice of formulation (displacement, velocity or acceleration) does not change the theoretical closed-loop stability properties defined by the loop-gain $L(s) = n(s, \theta_n)p(s, \theta_p)$, but allows flexibility in the choice of sensor and actuator. As well as providing a conceptual basis for this paper, the substructuring approach links to classical control system concepts useful for stability and robustness analysis. Details can be found elsewhere (Gawthrop et al., 2007, 2009; Wagg et al., 2008).

The substructuring formulation of Figure 1(a) assumes an inertia-like physical component driven by a force; as discussed by Gawthrop et al. (2005), compliance-like physical components can be treated by the formulation of Figure 2(a) where the external force F_0 is replaced by an external velocity v_0 and the three components are now connected by a common force, or **0**, junction. To distinguish this velocity-driven formulation from the force-driven formulation in Figure 1(a) an over-bar is used:

$$F = \bar{p}(s, \theta_p)(v_0 - v), \tag{3}$$

$$v = \bar{n}(s, \theta_n)F. \tag{4}$$

Using the definitions of Equations (3) and (4), the block diagram equivalent of Figure 2(a) is Figure 2(b). Once again, displacement and acceleration formulations are given by Figure 2(c) and 2(d), respectively.

3. Dynamically dual design

As already discussed, in this paper a vibration absorber attached to a system is considered. This vibration absorber, while based on a physical component thus ensuring that the system is passive, is implemented as a controller. This setup can be considered within the substructuring framework, with the vibration absorber forming **Num** and the system which the vibration absorber is attached being **Phy**. One possible absorber is the Den Hartog resonant vibration absorber, which is usually represented by a conventional mass–spring–damper schematic. However, as pointed out by Den Hartog (1985), and discussed in greater depth by Shearer et al. (1971), can equally well be described by an equivalent electrical circuit analogue.

Here, the use of DDVAs is proposed as a method for generating suitable **Num** dynamics. As discussed in Section 3.2, the resonant vibration absorber of Den Hartog (1985) is an example of a DDVA and provides the motivation for this approach. In formulating the DDVA approach the following features of the Den Hartog resonant vibration absorber are abstracted and generalised:

(1) it is a one-port[3] passive[4] physical system,
(2) it is causally compatible with the system, in that, the output velocity of the system provides the input to the absorber and the force output of the absorber provides the input to the system,
(3) there is a variable coupling parameter,
(4) the absorber has the *same* resonant frequency as the system, and
(5) the damping ratio of the absorber is *greater* than that of system.

The DDVA design approach is to set **Num** to be a dynamic-dual of the key mode or modes of the system that

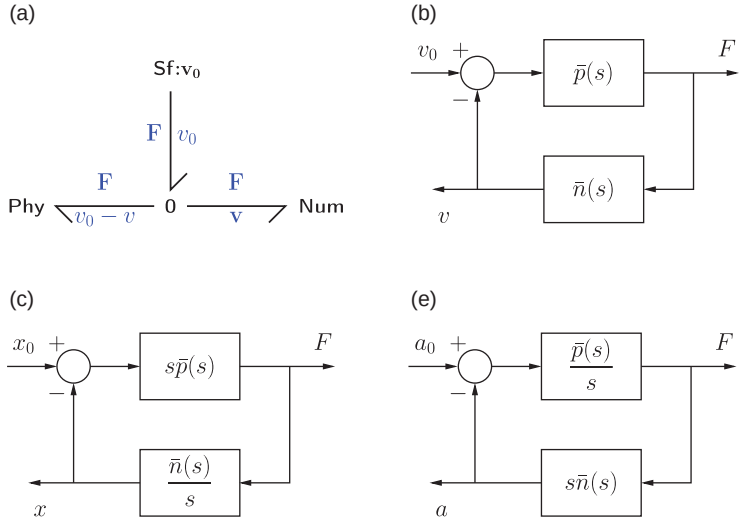

Figure 2. The velocity-driven substructuring formulation. (a) Bond graph, (b) block-diagram: velocity formulation, (c) block-diagram: displacement formulation and (d) block-diagram: acceleration formulation.

the absorber is attached to (which is contained in **Phy**). The method of obtaining a dynamic dual is now discussed. This is followed by discussions of two common absorber strategies which are DDVA; the Den Hartog absorber and the acceleration feedback method proposed by Preumont (2002).

3.1. *A dynamic-dual*

A dynamic-dual of a system is obtained by interchanging the rôles of velocity and force, is defined in Shearer et al. (1971). An extended version of this concept, the *scaled dual* is used here and, in the context of mechanical systems is defined as follows:

(1) Each force F_i, and each velocity v_i, in the original system has a scaled dual v_i^D, and F_i^D in the dual system given by:

$$v_i^D = \frac{1}{g}F_i, \tag{5}$$

$$F_i^D = g v_i, \tag{6}$$

where g is the scaling factor and $g = 1$ corresponds to the unscaled dual.

(2) Each mass component with mass m_i is replaced in the dual system with a spring component of stiffness K_i, each spring component with stiffness k_i is replaced in the dual system with a mass component of mass M_i, and each damper component with damping coefficient r_i is replaced in the dual system with a damper component with damping coefficient R_i where:

$$K_i = \frac{g^2}{m_i}, \tag{7}$$

$$M_i = \frac{g^2}{k_i}, \tag{8}$$

$$R_i = \frac{g^2}{r_i}. \tag{9}$$

(3) Common force connections become common velocity connections and common velocity connections become common force connections in the dual system.

(4) If the system transfer function $h(s)$ has force F as input and velocity v as output, then the dual transfer function $H(s)$ has velocity v^D as input and force F^D as output and is given by:

$$F^D = g v, \tag{10}$$

$$v^D = \frac{1}{g}F, \tag{11}$$

$$H(s) = \frac{F^D}{v^D} = \frac{gv}{(1/g)F} = g^2 h(s). \tag{12}$$

Equations (10) and (11) are *power conserving* in the sense that

$$F^D v^D = F v. \tag{13}$$

As these Equations (10) and (11) also interchange the roles of force and velocity, they correspond to the bond graph *gyrator* (**GY**) component of Figure 3.

Equations (7) and (8) ensure that the scaled dual retains the same natural frequencies as the system; in the sequel, the value R_i given using Equation (9) is not used, instead it

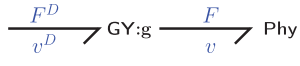

Figure 3. Gyrator interpretation of dynamic-dual.

is replaced by the user-selected value R'_i. This allows the damping of the modified scaled dual system, which forms the controller implemented in **Num**, to be adjusted.

Although not essential to the approach of this paper, the bond graph formulation provides a clear exposition of the notion of a scaled dual. In particular, the scaled dual system can be described in two different but equivalent ways as:

(1) the bond graph dual where the component moduli are given by Equations (7)–(9) or
(2) following Equation (13), the system obtained by appending a gyrator of modulus g to the system **Phy** port as in Figure 3. This point is also discussed by Gawthrop et al. (2010).

3.2. *Den Hartog absorber*

In his classical text book (Den Hartog, 1985, Section 3.3), Den Hartog considers the design of a damped vibration absorber for an undamped mass–spring system which is subject to a force disturbance. The specifications

(1) 'the main mass is 20 times greater than the damper mass',
(2) 'the frequency of the damper is equal to the frequency of the main system',
(3) The damping ratio of the damper is $\zeta = 0.1$.

were considered.

In the terminology used in this paper, the physical system requiring vibration suppression (**Phy**) is the undamped mass–spring oscillator. In Den Hartog (1985) the vibration absorber was considered to be a physical mechanical device but here it is considered to be a controller (with sensor and actuator) with the same dynamics as the absorber and forms **Num**. The disturbance force acts on the undamped mass–spring oscillator **Phy**, as does a force due to the presence of the absorber **Num**, therefore the system can be represented by the block diagram given in Figure 1(b).

Figure 4(b) and 4(a) gives the schematic diagram of the damped vibration absorber **Num** and the undamped oscillator **Phy**, respectively. A damper with $r = \infty$ is included in the subsystem **Phy** of Figure 4(a) to allow for the corresponding component in the subsystem **Num**. Using standard manipulations, the transfer function of the physical system, **Phy**, of Figure 4(a) is:

$$p(s,\theta_p) = \frac{s(ms+r)}{mrs^2 + kms + kr}. \tag{14}$$

Letting $r \to \infty$ gives:

$$p(s,\theta_p) = \frac{s}{ms^2 + k}. \tag{15}$$

Similarly, from Figure 4(b), the transfer function for **Num**, which represents the Den Hartog absorber, is

$$n(s,\theta_n) = \frac{Ms(Rs+K)}{Ms^2 + Rs + K}. \tag{16}$$

It can be shown that this absorber is a scaled dynamic-dual of the system, **Phy**, it is applied to. Considering the system **Phy**, given in Equation (14), and applying the dual transforms, given in Equations (7)–(9), the parameters m, k and r can be rewritten in terms of M,K and D to give:

$$\begin{aligned} &p(s,\theta_p) \\ &= \frac{s((g^2/k)s + (g^2/R))}{(g^2/k)(g^2/R)s^2 + (g^2/M)(g^2/K)s + (g^2/M)(g^2/R)} \\ &= \left(\frac{1}{g^2}\right)\frac{Ms(Rs+K)}{Ms^2 + Rs + Kr}. \end{aligned} \tag{17}$$

Applying the scaling given in Equation (12), the scaled dual of **Phy** is

$$P(s,\Theta_p) = g^2 p(s,\theta_p) = \frac{Ms(Rs+K)}{Ms^2 + Rs + Kr}. \tag{18}$$

Thus, by comparing this to Equation (16), it can be seen that the Den Hartog absorber in **Num** corresponds to the scaled dual of **Phy**:

$$n(s,\theta_n) = P(s,\Theta_p). \tag{19}$$

The first part of the Den Hartog specifications is achieved by setting:

$$M = \alpha m \quad \text{where } \alpha = \frac{1}{20}. \tag{20}$$

The second part of the specification is achieved by setting

$$\frac{K}{M} = \frac{k}{m}. \tag{21}$$

Equations (20) and (21) imply that

$$K = \alpha k. \tag{22}$$

Moreover, using Equations (7) and (22), the scaling gain g is given by

$$g^2 = Km = \alpha mk. \tag{23}$$

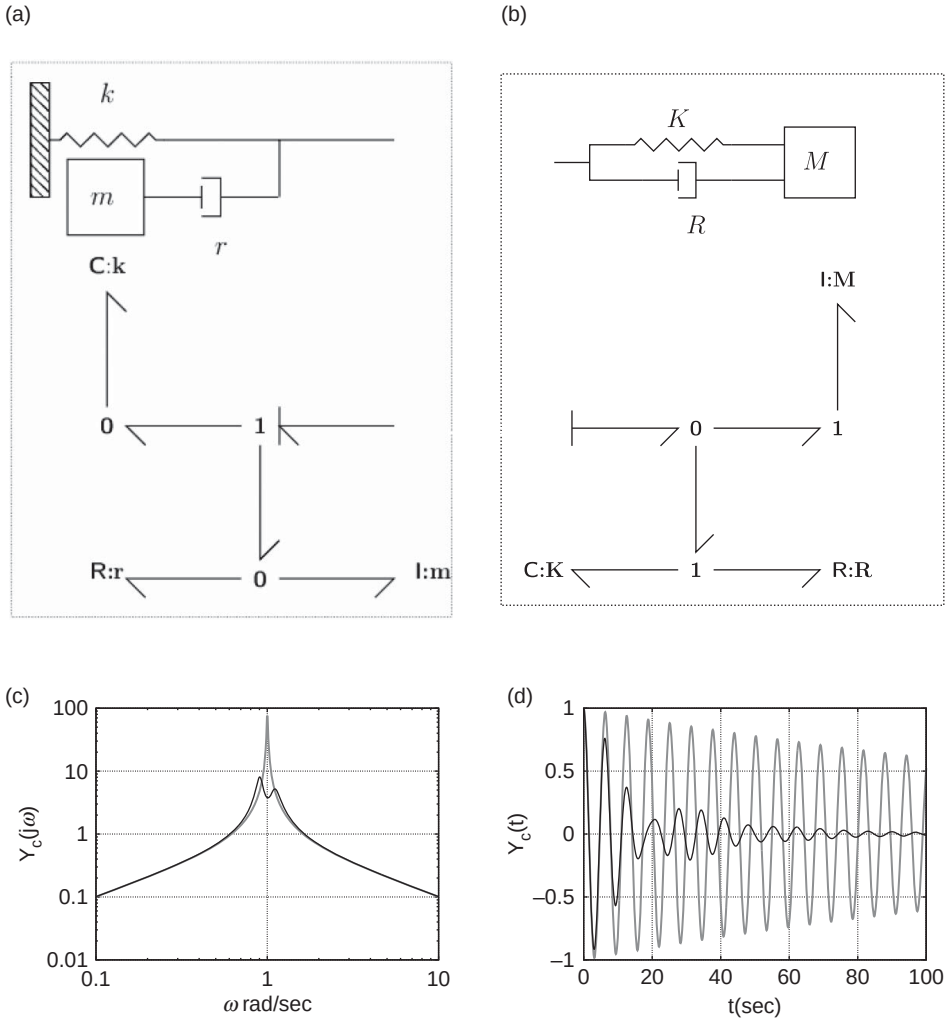

Figure 4. Den Hartog absorber. The physical system (a) and its vibration absorber (and dynamic-dual) (b) are first-order mass–spring—damper systems. (c) The closed-loop frequency response (black line) has a lower resonant peak than the open-loop response (grey line). (d) The closed-loop impulse response (black line) exhibits more damping than the open-loop impulse response (grey line). (a) **Phy**: the physical system, (b) **Num**: the dual physical system, (c) frequency response $H(j\,\omega)$ and (d) impulse response $h(t)$.

Finally, the third part of the specification is achieved by replacing the damping coefficient R of $n(s, \theta_n)$ by

$$R' = 2\zeta\sqrt{MK}. \tag{24}$$

To illustrate the properties of this particular vibration absorber, the unit system with $m = k = 1$ was used. Using the specification described above, this gives the numerical system parameters $M = K = 0.05$ and $R' = 0.01$, and so the DDVA is given by:

$$n(s, \theta_n') = \frac{Ms(R's + K)}{Ms^2 + R's + K} = \frac{0.01s^2 + 0.05s}{s^2 + 0.2s + 1}. \tag{25}$$

The corresponding closed-loop frequency response appears in Figure 4(c); this shows the 'split peak' phenomenon described by Den Hartog (1985). The corresponding closed-loop impulse response appears in Figure 4(d); this decays exponentially over the time scales determined by the specified damping ratio.

3.3. *Acceleration feedback*

The acceleration feedback method has been proposed by Preumont (2002). This section rederives the algorithm from the DDVA point of view. In particular, the undamped physical system of Figure 4(a) (with $1/r = 0$) can equally well be represented in Figure 5(a) with $r = 0$. This system has a different modified dual and thus gives a different form of control; this turns out to be a form of acceleration feedback.

As with the last example the vibration absorber is acting on an undamped mass–spring oscillator. The undamped oscillator forms **Phy** as shown in Figure 5(a). Note that a damper with $r = 0$ is included to allow a dynamic-dual to be formulated. Using standard manipulations, the transfer function of the physical system **Phy** of Figure 5(a) is

$$p(s, \theta_p) = \frac{s}{ms^2 + rs + k}. \tag{26}$$

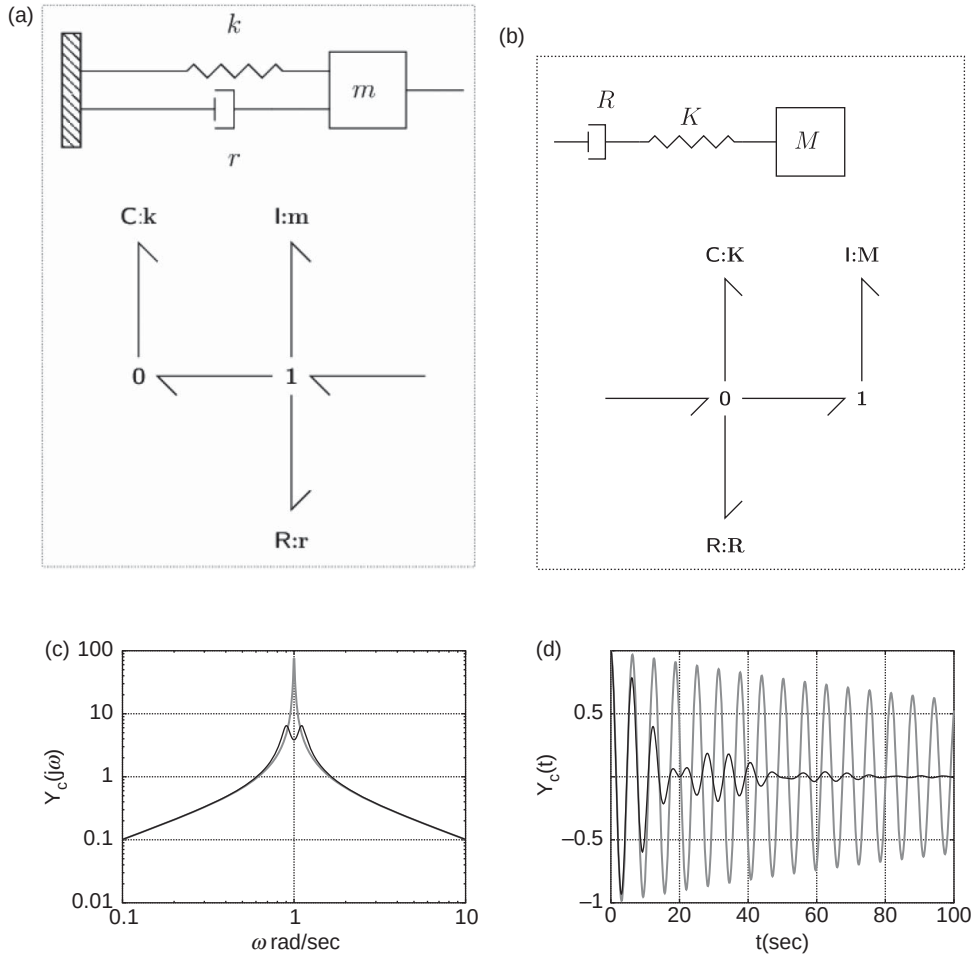

Figure 5. Acceleration feedback. Like the Den Hartog absorber of Figure 4, the physical system and the dual are mass–spring–damper systems, but the configuration is different. The closed and open-loop responses are similar to those of the Den Hartog absorber of Figure 4, but the split peaks are more symmetrical. (a) **Phy**: the physical system, (b) **Num**: the dual physical system, (c) frequency response $H(j\,\omega)$ and (d) impulse response $h(t)$.

Setting $r = 0$ gives

$$p(s, \theta_p) = \frac{s}{ms^2 + k}. \tag{27}$$

The controller transfer function, forming **Num**, for the acceleration feedback method (Preumont, 2002) is given by

$$n(s, \theta_n) = g^2 p(s, \theta_p) = \frac{g^2 s}{ms^2 + rs + k}. \tag{28}$$

Using Equation (12), it can be seen that the numerical system **Num** is the scaled dynamic-dual of **Phy**. Figure 5(b) gives a physical representation of the acceleration feedback controller, where the component values R, K and M can be calculated using Equations (7)–(9) but are not required.

To give a direct comparison with Section 3.2, the same system and design considerations are used to give the DDVA:

$$n(s, \theta_n') = \frac{0.05s}{s^2 + 0.2s + 1}. \tag{29}$$

This is similar to the DDVA of Equation (25) except that the numerator s^2 term is not present.

The corresponding closed-loop frequency response appears in Figure 5(c); this is similar to Figure 4(c) except that the peaks have a more similar amplitude. The corresponding closed-loop step response appears in Figure 5(d); again, this decays exponentially over the time scales determined by the specified damping ratio.

4. Systems with multiple modes of vibration

The examples discussed in the previous section demonstrate that the DDVA approach gives the same type of vibration absorber for the well known cases associated with mass–spring–damper systems. The real advantage of the DDVA approach is when using it to reduce vibrations in systems with multiple modes of vibration. The steps involved are the same as above: (i) define a physical model of the system **Phy**, (ii) set **Num** as the modified scaled dual of **Phy**, and (iii) connect the systems via a single (one-port) connection. As discussed in Section 3.1, step (ii) can either be accomplished directly or indirectly using the **GY** approach of Figure 3. In this paper, attention is focused

Table 1. Modal system: resonant frequencies.

n	ω_n (rad/s)
1	1.0
2	2.0

on linear models thus giving rise to transfer-function representations.

Two examples are considered here. The first is a two degree-of-freedom lumped mass system which is shown schematically in Figure 6(a) and 6(b). Figure 6(a) and 6(b) are similar to Figure 5(a) and 5(b) except that there are *two* coupled mass–spring damper systems involved. Thus **Phy** can be regarded as the modal decomposition of a 2DOF system and **Num** the corresponding vibration absorber. For the purposes of illustration, each subsystem of **Num** has the same parameters as in the example of Figure 5 of Section 3.3 (Table 1).

Figure 6(c) shows the open (without the vibration absorber) and closed-loop (with the vibration absorber) frequency response magnitudes. The magnitude of the closed-loop response (black line) is clearly smaller than the corresponding open-loop response (grey line) at the two resonant frequencies. Figure 6(d) shows the equivalent impulse response; as predicted by the frequency responses, the closed-loop impulse response decays more rapidly than the equivalent open-loop response.

As a second example, a uniform Euler-Bernoulli[5] cantilever beam (with one end fixed and the other free) modelled using a 10 element, finite-element bond graph model (Karnopp, Margolis, & Rosenberg, 2000; Margolis, 1985) is considered. Such beam models are undamped; but the DDVA approach needs to include damping in **Num**. For the purposes of this example, Rayleigh damping is assumed; in particular, each compliant element in the lumped model has an associated damping term represented by a damper connected across the ends of the compliant elements.

Following Balas (1978, Section V) who considers a 'unit beam', the cantilever beam is normalised to have unit mass per unit length and unit compliance per unit length. **Phy** is assumed to have a small (but non-zero) damping of 10^{-6} per unit length. The 10 modal frequencies appear in Table 2. For the purposes of illustration, the vibration absorber was applied to the beam using a collocated point Force/Velocity actuator/sensor halfway along the beam. As discussed in the sequel, this point corresponds to a nodal point of the third-resonance and thus this mode cannot be controlled with this choice. The choice of actuator/sensor location is an interesting topic not considered in this paper.

Two versions of DDVA were used. The first DDVA was obtained by considering the complete dynamic-dual of **Phy**. The scaled dual **Num** was obtained using the **GY** approach of Figure 3. A feature of this approach is that

Table 2. Cantilever beam model modal frequencies.

n	ω_n (rad/s)
1	2.919
2	18.28
3	50.37
4	95.59
5	150.4
6	210.0
7	269.1
8	322.0
9	363.9
10	390.8

Note: Not all frequencies appear in Figures 7 and 8 due to coincident zeros.

there are only two control parameters. These were chosen as the gyrator gain $g^2 = 0.05$ and the damping of the cantilever beam model in **Num** as 2 per unit length.

Figure 7(a) shows the open (without the vibration absorber) and closed-loop (with the vibration absorber) frequency response magnitudes. This figure has been expanded to show the frequency responses close to the first–fourth resonances in Figure 7(c)–7(f), respectively. Near the first two resonances (Figure 7(c) and 7(d)), the magnitude of the closed-loop response (black line) is clearly smaller than the corresponding open-loop response (grey line) at the two resonant frequencies. The third resonance corresponds to a node at the sensor/actuator and the fourth is well damped anyway. Thus this controller design naturally applies control authority at the important resonances. Figure 7(b) shows the equivalent impulse response; as predicted by the frequency responses, the closed-loop impulse response decays more rapidly than the equivalent open-loop response. As noted above, the third resonance is not controlled using this approach. However, it could be controlled either by moving the sensor/actuator away from the node or by having a second sensor/actuator away from the node.

The second approach is to use the scaled dynamic-dual of a two mode modal model (as in Figure 6(b)), capturing the dynamics of the first two modes of the cantilever. This is then connected to the same cantilever beam. The parameters of **Num** are the same as in the example of Figure 6 and those of **Phy** the same as those of the example of Figure 7.

Figure 8(a) shows the open (without the vibration absorber) and closed-loop (with the vibration absorber) frequency response magnitudes. This figure has been expanded to show the frequency responses close to the first–fourth resonances in Figure 8(c)–8(f), respectively. Near the first two resonances (Figure 8(c) and 8(d)), the magnitude of the closed-loop response (black line) is clearly smaller than the corresponding open-loop response (grey line) at the two resonant frequencies; these Figures are not the same as Figure 7(c) and 7(d) because

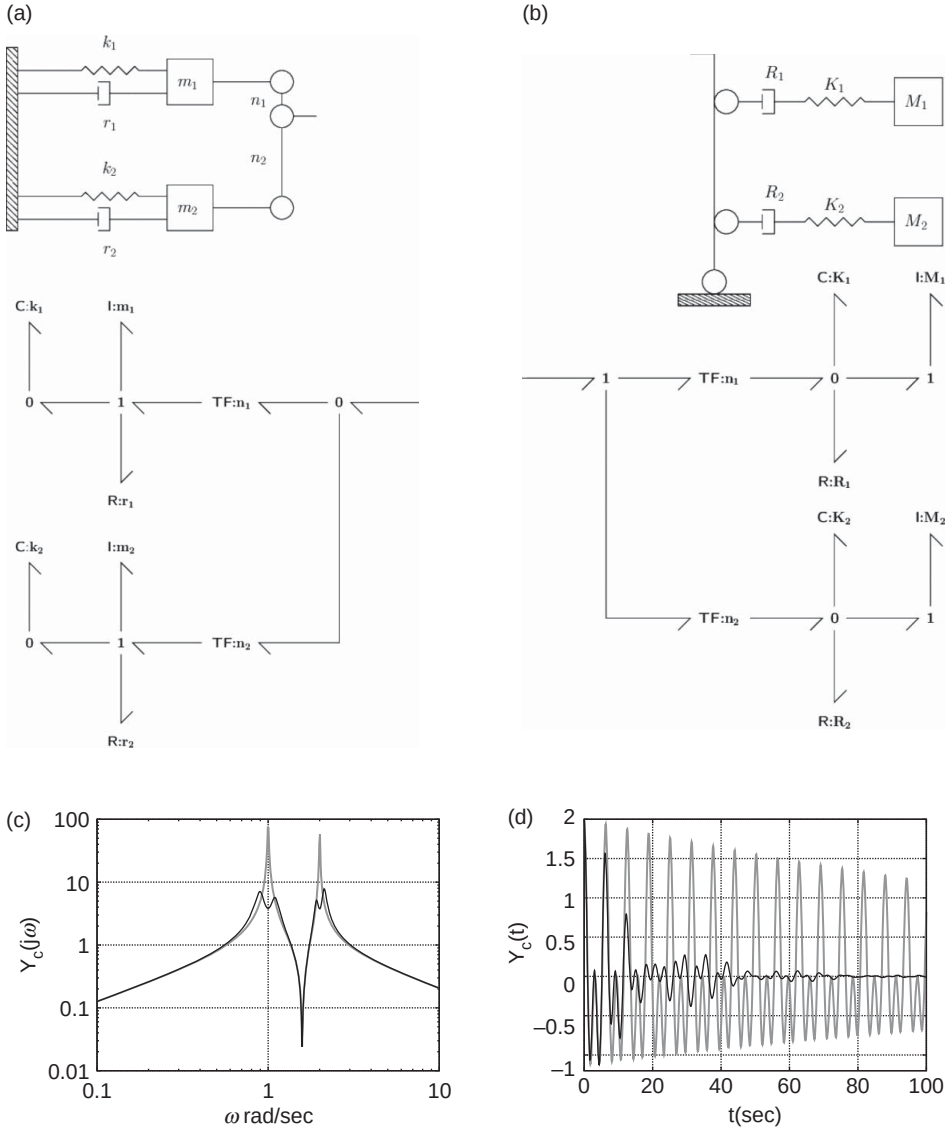

Figure 6. Modal system. Both the physical system and its dual are coupled mass–spring–damper systems and are thus fourth-order. (c) The closed-loop frequency response (black line) has both resonant peaks lower than the open-loop response (grey line). (d) Again, the closed-loop impulse response (black line) exhibits more damping than the open-loop impulse response (grey line). (a) **Phy**: the physical system, (b) **Num**: the dual physical system, (c) frequency response $H(j\omega)$ and (d) impulse response $h(t)$.

the controller is different; but the effect is similar. The third and fourth resonances are explicitly not controlled with this method; but, in this case, the effect is the same as that of the controller of the example of Figure 7. In particular Figure 8(b) shows that the closed-loop impulse response decays more rapidly than the equivalent open-loop response in a similar fashion to that of Figure 7(b). In this particular example, the performance of the two controllers is quite similar.

5. Experimental results

As indicated in Figure 9, the experiments were based on the Quanser (Apkarian, 1995) SRV02 rotational servo-motor and associated UPM-15-03-240 power and instrumentation module. The SRV02 was firmly clamped to a rigid bench and interfaced to a Intel CoreTM 2 Duo Processor (2.66 GHz) based computer via a National Instruments PCI-8024E analogue-digital conversion card and cable and the corresponding Quanser interface board.

In the experiment described here, the computer used the real-time Linux operating system RTAI together with the control-orientated software RTAI-Lab (Bucher & Balemi, 2006) running at a sampling frequency of 500 Hz. Using this software, the SRV02 rotational servo motor, rotational position sensor and associated power supply were controlled to give high-gain position control using a proportional and derivative (PD) controller. The servo angle was measured using a potentiometer and scaled within the computer to measure angular position in radians.

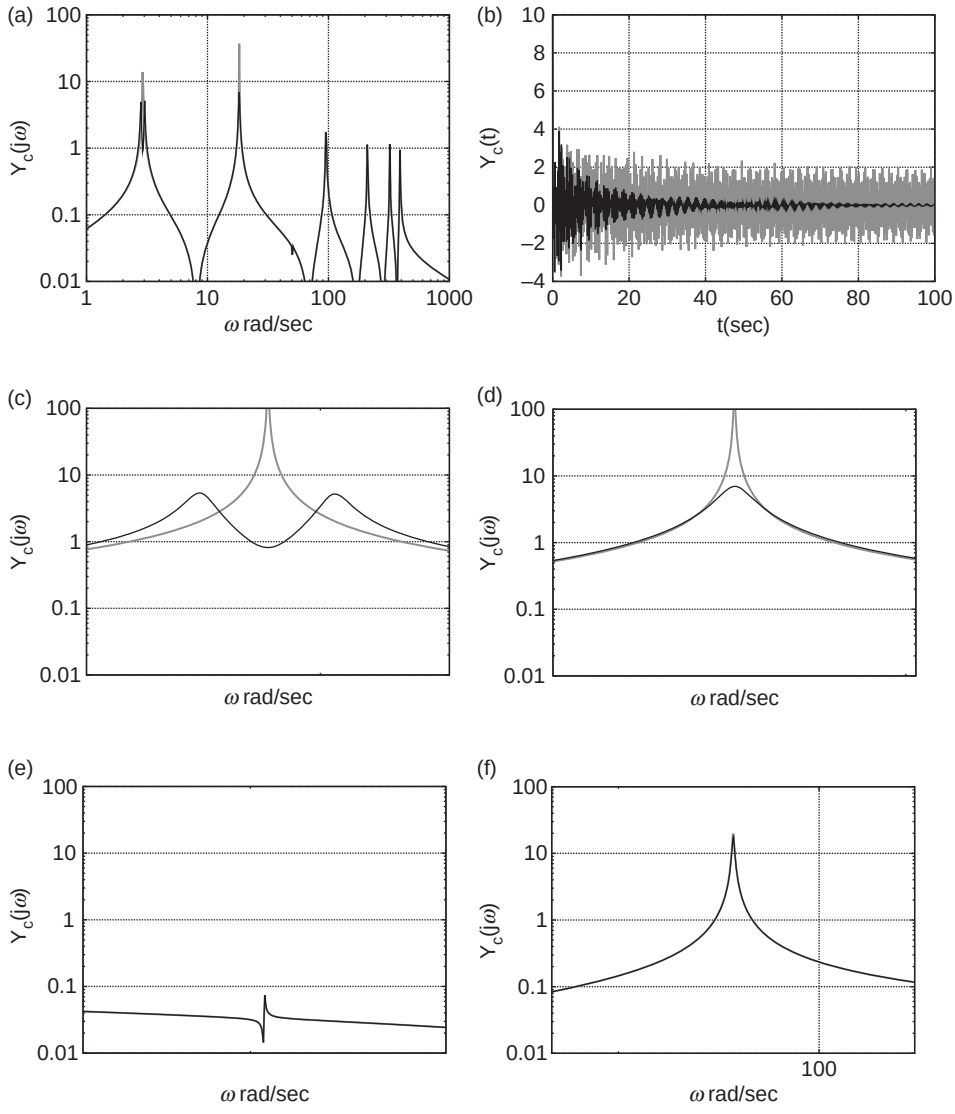

Figure 7. Cantilever beam with dual feedback. (a) Frequency responses $H(j\omega)$, (b) impulse responses $h(t)$, (c) $H(j\omega)$ – first resonance, (d) $H(j\omega)$ – second resonance, (e) $H(j\omega)$ – third resonance and (f) $H(j\omega)$ – fourth resonance.

5.1. *Flexible joint*

The Quanser cantilever beam experiment (Apkarian, 1995) has two parts that may be considered using the substructuring configuration shown in Figure 2(c). The physical component, **Phy**, consists of a rigid arm which is mounted to a platform via a pivot. This pivot exhibits a stiffness due to two linear springs mounted between the platform and the arm. A position disturbance is provided to the system via the rotational servo motor on which the platform is mounted (the pivot is directly above the motor). The vibration absorber, **Num**, has a torque input F. Because of the springs in **Phy**, this torque is proportional to the joint deflection angle θ (the arm rotation relative to the platform rotation), and so is generated from this measurement. The output of **Num** is a rotational displacement x which, along with the disturbance x_0, is imposed on **Phy** using the servo motor by setting the servo motor PD controller demand to $x_0 - x$ (Figure 10).

The open-loop properties of the system were investigated by applying a square-wave reference signal with a period of 10 s to the servo and measuring both the servo angle x_a and the joint angle θ for 5 periods. Because all of the signals are periodic, the methods of Pintelon & Schoukens (2001) were used to generate the frequency response of the system at the discrete frequencies corresponding to the periodic input. Figure 11 gives two measured frequency responses:

(1) $+$ indicates the response from servo angle x_a to joint angle θ.
(2) $\circ$ indicates the response from servo reference to θ.

These responses match at low frequencies, but the gain of the second transfer function falls at the higher frequencies due to the limited servo bandwidth of about 10 Hz.

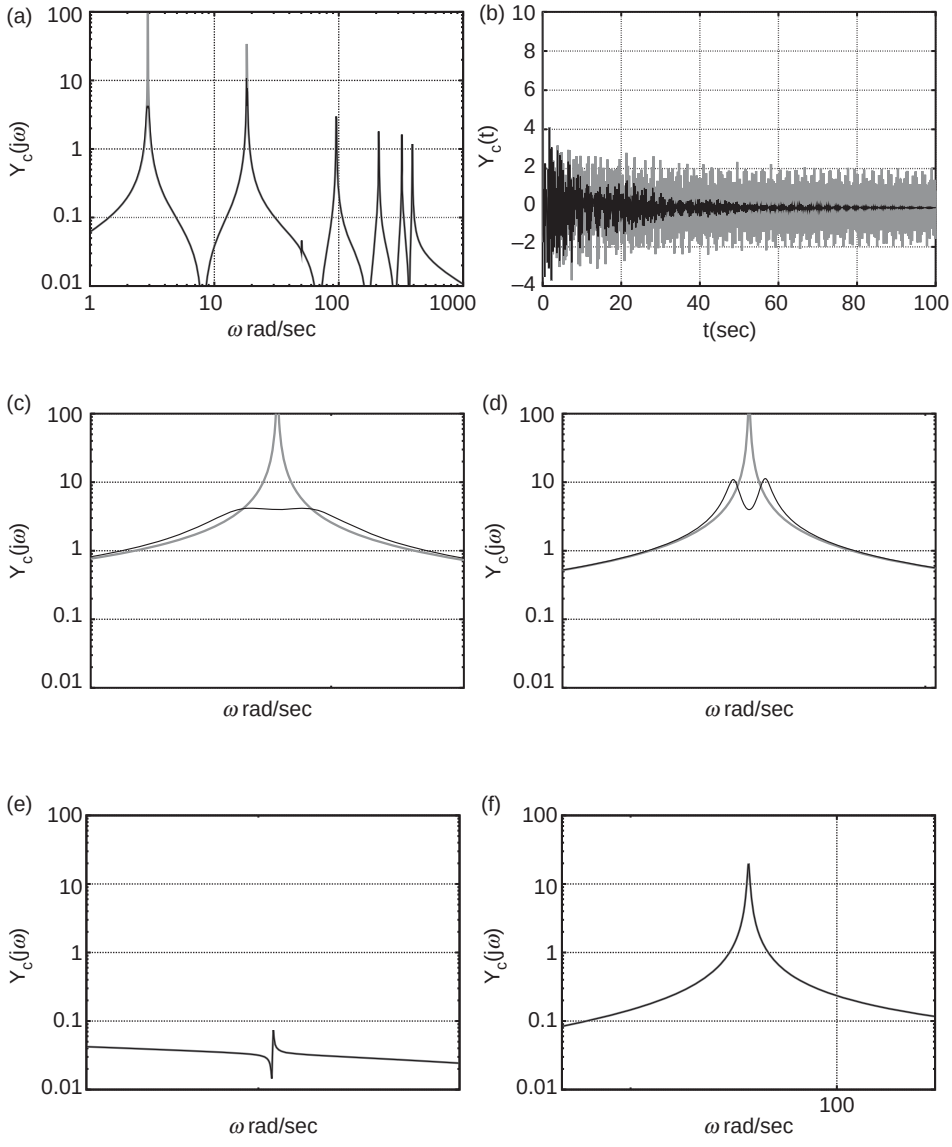

Figure 8. Cantilever with dual modal feedback. (a) Frequency responses $H(j\,\omega)$, (b) impulse responses $h(t)$, (c) $H(j\,\omega)$ – first resonance, (d) $H(j\,\omega)$ – second resonance, (e) $H(j\,\omega)$ – third resonance and (f) $H(j\,\omega)$ – fourth resonance.

With reference to Figures 2(c) and 10(a) the physical system **Phy** relating input displacement to output force is of the form

$$s\bar{p}(s,\theta_p) = \frac{g_0 s^2}{s^2 + 2\xi_0\omega_0 s + \omega_0^2}. \tag{30}$$

The parameters θ_p were fitted to the first measured frequency response with $\omega_0 = 15.1\,\text{rad}\,s^{-1}$ and $\xi_o = 0.02$.

Following the methodology of Section 3.3 in the dual version of Figure 2(c), the feedback transfer function was chosen to be of the form:

$$\frac{\bar{n}(s,\theta_n)}{s} = \frac{g_c}{s^2 + 2\xi_c\omega_0 s + \omega_0^2}, \tag{31}$$

where $g_c = g^2 g_0$ is a variable positive gain factor and the damping ratio $\xi_c = 0.3$.

The periodic input experimental method described above was used. Figure 12 shows the experimental frequency results for three values of g_c: $g_c = 0$, $g_c = 20$, and $g_c = 40$. $g_c = 0$ corresponds to Figure 11. The height of the resonant peak is reduced in the two non-zero cases and the peak splitting of Figure 5(c) is evident in Figure 12 for the highest gain of $g_c = 40$. Figure 13 shows the periodic data corresponding to the joint angle θ for the three gain values. The five consecutive periods have been superimposed to form the figures; the variability between periods is essentially high-frequency noise. As indicated by the frequency responses, the time responses show damping increasing with gain.

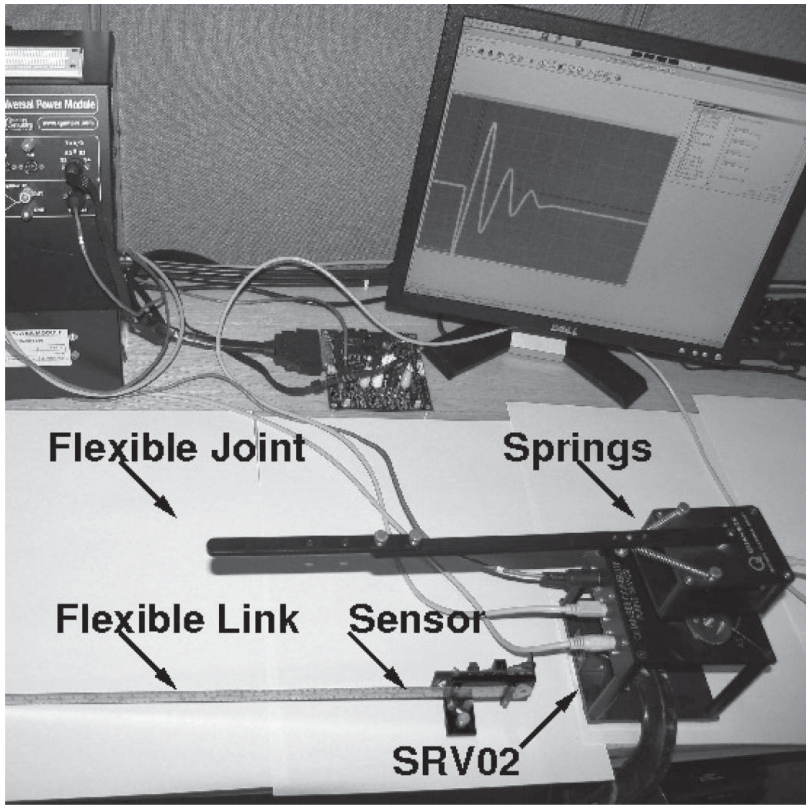

Figure 9. Experimental systems. Experimental systems. The SRV02 servomotor module is in the bottom right-hand corner and the associated power module in the top left-hand corner. The computer display is at the top right and the computer interface board near the centre. The flexible joint module is shown mounted on the SRV02 and rotates about a vertical axis driven though the two springs. The cantilever beam module is shown unmounted and replaces the flexible joint module in the second set of experiments.

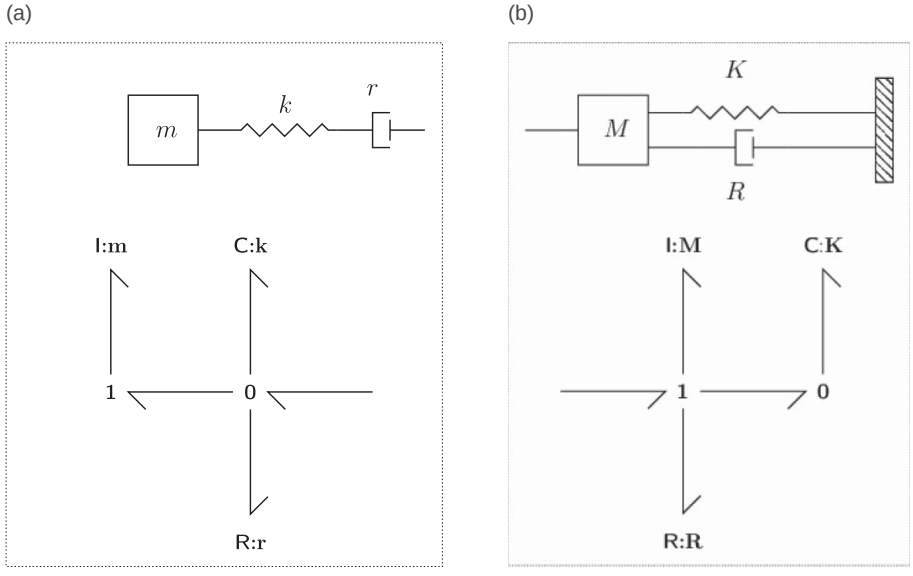

Figure 10. Rotational joint experiment. (a) With the components interpreted in a rotational sense and $r \to \infty$, **Phy** represents the rotating arm with the attached springs. (b) **Num** is the modified scaled dual of **Phy**. (a) **Phy**: the physical system and (b) **Num**: the dual physical system.

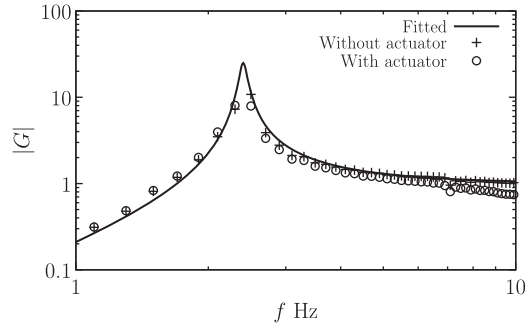

Figure 11. Flexible joint: open-loop frequency responses. Flexible joint: open-loop frequency responses. + indicates the response from servo angle x to joint angle θ; ○ indicates the response from servo reference to θ. The solid line is the fitted frequency response.

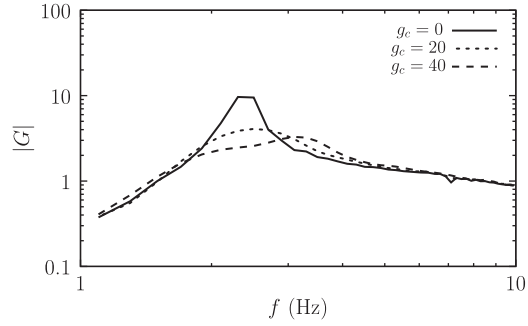

Figure 12. Flexible joint: closed-loop frequency responses.

5.2. *Cantilever beam*

The flexible joint module was replaced by the cantilever beam module in Figure 9. A strain gauge measures the curvature at the root of the cantilever beam. In the same way as the joint potentiometer of Section 5.1 provided a voltage proportional to torque F, the strain gauge sensor provides a voltage proportional to torque F. The open-loop response was measured using the same methods. Two resonances and one anti-resonance appear in the measured frequency response and similarly to Section 5.1, this was fitted by a transfer function of the form:

$$s\bar{p}(s,\theta_p) = g_0\left[\frac{\kappa_1 s^2}{s^2 + 2\xi_1\omega_1 s + \omega_1^2} + \frac{\kappa_2 s^2}{s^2 + 2\xi_2\omega_2 s + \omega_2^2}\right] \tag{32}$$

with $\omega_1 = 23.25\,\text{rad}\,\text{s}{-}1$,$\omega_2 = 159.00\,\text{rad}\,\text{s}{-}1$, $\xi_1 = \xi_2 = 0.04$, $\kappa_1 = 0.36$ and $\kappa_2 = 1 - \kappa_1 = 0.64$. Because of the 10 Hz servo bandwidth, the discrepancy between measured and fitted transfer function is large above 10 Hz.

Following the methodology of Section 4 a two-mode transfer function corresponding to Equation (33) was

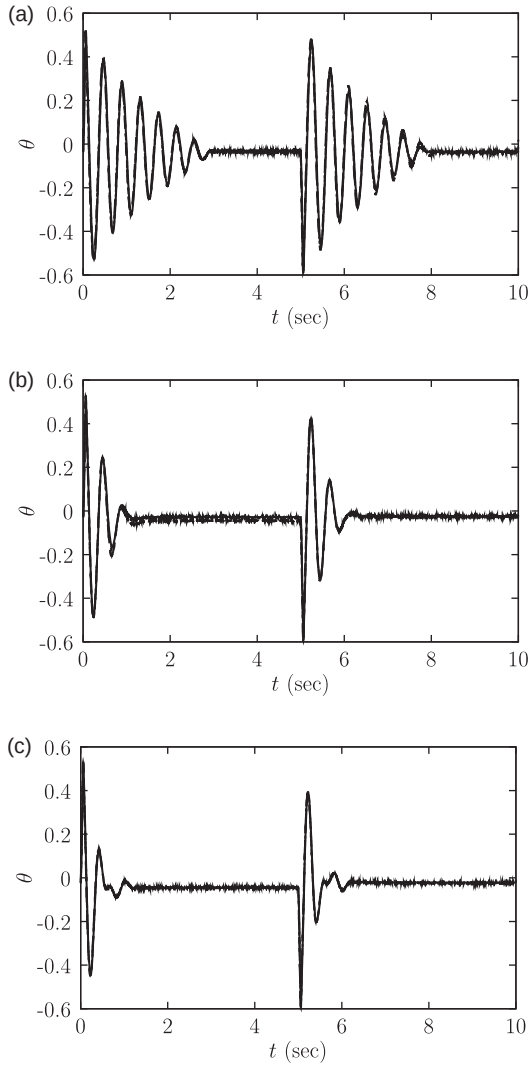

Figure 13. Flexible joint: time responses. (a) $g_c = 0$, (b) $g_c = 20$ and (c) $g_c = 40$.

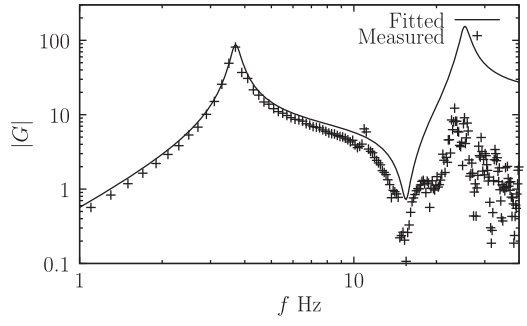

Figure 14. Cantilever beam: open-loop frequency responses. Cantilever beam: open-loop frequency responses. + indicates the response from servo angle x to joint angle θ. The firm line is the fitted frequency response.

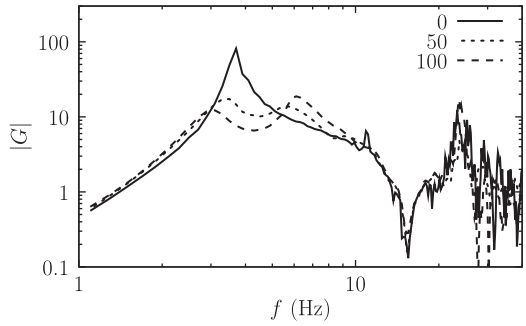

Figure 15. Cantilever beam: closed-loop frequency responses for the cases where $g_c = 0$, 50 and 100.

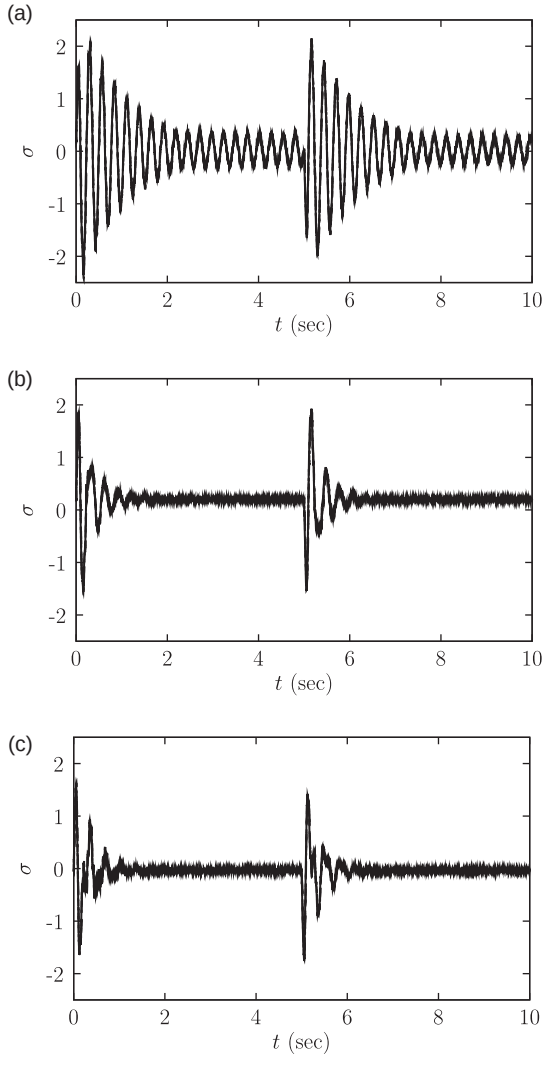

Figure 16. Cantilever beam: time responses. (a) $g_c = 0$, (b) $g_c = 50$ and (c) $g_c = 100$.

chosen as:

$$\frac{\bar{n}(s,\theta_n)}{s} = g_c\left[\frac{\kappa_1 s^2}{s^2 + 2\xi_c\omega_1 s + \omega_1^2} + \frac{\kappa_2 s^2}{s^2 + 2\xi_c\omega_2 s + \omega_2^2}\right] \tag{33}$$

with $\xi_c = 0.3$.

The periodic input experimental method described above was used. Figure 15 shows the experimental frequency results for three values of g_c: $g_c = 0$, $g_c = 50$, and $g_c = 100$. $g_c = 0$ corresponds to Figure 14. The height of the first resonant peak is reduced in the two non-zero cases and the peak splitting of Figure 8(a) is evident in Figure 15 for both cases. The second resonance is largely unaffected; we attribute this to the limited actuator bandwidth. Figure 16 shows the periodic data corresponding to the measured strain voltage σ for the three gain values. As with Figure 13, five consecutive periods have been superimposed to form the figures showing that the variability between periods is essentially high-frequency noise. Again, as indicated by the frequency responses, the time responses show damping increasing with gain.

6. Conclusion

The DDVA approach has been shown to provide a novel method to design vibration absorbers in the physical domain. In particular, the method is a natural generalisation of not only the classical single-degree of freedom vibration absorber of Den Hartog (1985, Section 3.3) but also of acceleration feedback (Preumont, 2002). Placing these two well-known design methods into the wider context of the DDVA of this paper has the following advantages: the methods immediately extend to multi degree of freedom systems and the implementation and theoretical results (including robustness to sensor/actuator dynamics) from substructuring can be directly applied.

The DDVA approach has been illustrated using numerical simulations of single mode and multi-mode systems and verified using two experimental systems: a rigid beam with an flexible joint and a flexible cantilever beam. Future work will apply the results to more complex dynamical systems including those with multiple sensor-actuator pairs.

The location of the sensor-actuator pairs has not been considered in this paper even though it certainly affects controllability and observability issues (Balas, 1978). Future work in this area will extend bond graph approaches (for example those of Marquis-Favre & Jardin (2011) and Gawthrop & Rizwi (2011)) to sensor/actuator placement in this context.

In principle, the method is equally applicable to the control nonlinear vibrations where dynamical dual of the nonlinear physical system provides the basis for a nonlinear controller. This is also an area for future work.

Acknowledgements

Peter Gawthrop was a Visiting Research Fellow at The University of Bristol when this work was accomplished; he is now supported by a Professorial Fellowship at the University of Melbourne.

Disclosure statement

No potential conflict of interest was reported by the authors.

Funding

Simon Neild is supported by EPSRC fellowship EP/K005375/1. David Wagg is supported by EPSRC [grant EP/K003836/2].

Notes

1. As the word 'dual' has many meanings, the term dynamically dual is used for the specific meaning of this paper.
2. The bond directions have been changed for this paper to correspond to the usual sign convention for feedback control block diagrams.
3. 'One-port' refers to the single *energy port* associated with force and velocity
4. In the sense that it consumes but does not produce energy.
5. Other models such as the Timoshenko model, as well as non-uniform beams, could similarly be handled using this approach

References

Ali, S. F., & Padhi, R. (2009). Active vibration suppression of non-linear beams using optimal dynamic inversion. *Journal of Systems and Control Engineering*, *223*(5), 657–672.

Anderson, B. D. O., & Vongpanitlerd, S. (2006). *Network analysis and synthesis a modern systems theory approach*. Dover. First published 1973 by Prentice-Hall.

Apkarian, J. (1995). *A comprehensive and modular laboratory for control systems design and implementation*. Markham, Ontario: Quanser Consulting.

Balas, M. J. (1978). Feedback control of flexible systems. *IEEE Transactions on Automatic Control*, *23*(4), 673–679.

Blakeborough, A., Williams, M. S., Darby, A. P., & Williams, D. M. (2001). The development of real-time substructure testing. *Philosophical Transactions of the Royal Society Part A*, *359*, 1869–1891.

Borutzky, W. (2011). *Bond graph modelling of engineering systems: Theory, applications and software support*. New York, NY: Springer.

Bucher, R., & Balemi, S. (2006). Rapid controller prototyping with matlab/simulink and linux. *Control Engineering Practice*, *14*(2), 185–192.

Cellier, F. E. (1991). *Continuous system modelling*. Berlin: Springer-Verlag.

Den Hartog, J. P. (1985). *Mechanical vibrations*. Dover. Reprint of 4th ed. Published by McGraw-Hill 1956.

Desoer, C. A., & Vidyasagar, M. (1975). *Feedback systems: Input-output properties*. London: Academic Press.

Fleming, A. J., & Moheimani, S. O. R. (2005). Control oriented synthesis of high-performance piezoelectric shunt impedances for structural vibration control. *IEEE Transactions on Control Systems Technology*, *13*(1), 98–112.

Gawthrop, P. J. (1995). Physical model-based control: A bond graph approach. *Journal of the Franklin Institute*, *332B*(3), 285–305.

Gawthrop, P. J. (2004). Bond graph based control using virtual actuators. *Proceedings of the Institution of Mechanical Engineers Pt. I: Journal of Systems and Control Engineering*, *218*(4), 251–268.

Gawthrop, P. J., & Bevan, G. P. (2007). Bond-graph modeling: A tutorial introduction for control engineers. *IEEE Control Systems Magazine*, *27*(2), 24–45.

Gawthrop, P. J., & Rizwi, F. (2011). Coaxially coupled inverted pendula: Bond graph-based modelling, design and control. In W. Borutzky (Ed.), *Bond graph modelling of engineering systems* (pp. 179–194). New York, NY: Springer.

Gawthrop, P. J., & Smith, L. P. S. (1996). *Metamodelling: Bond graphs and dynamic systems*. Hemel Hempstead: Prentice Hall.

Gawthrop, P. J., Bhikkaji, B., & Moheimani, S. O. R. (2010). Physical-model-based control of a piezoelectric tube for nano-scale positioning applications. *Mechatronics*, *20*(1), 74–84. Available online 13 October 2009.

Gawthrop, P. J., Wagg, D. J., & Neild, S. A. (2009). Bond graph based control and substructuring. *Simulation Modelling Practice and Theory*, *17*(1), 211–227. Available online 19 November 2007.

Gawthrop, P. J., Wallace, M. I., Neild, S. A., & Wagg, D. J. (2007). Robust real-time substructuring techniques for under-damped systems. *Structural Control and Health Monitoring*, *14*(4), 591–608. Published on-line: 19 May 2006.

Gawthrop, P. J., Wallace, M. I., & Wagg, D. J. (2005). Bond-graph based substructuring of dynamical systems. *Earthquake Engineering & Structural Dynamics*, *34*(6), 687–703.

Hagood, N. W., & von Flotow, A. (1991). Damping of structural vibrations with piezoelectric materials and passive electrical networks. *Journal of Sound and Vibration*, *146*(2), 243–268.

Hogan, N. (1985). Impedance control: An approach to manipulation. part I – theory. *ASME Journal of Dynamic Systems, Measurement and Control*, *107*, 1–7.

Høgsberg, J. R., & Krenk, S. (2006). Linear control strategies for damping of flexible structures. *Journal of Sound and Vibration*, *293*(1–2), 59–77.

Hong, J. H., & Bernstein, D. S. (1998). Bode integral constraints, colocation, and spillover in active noise and vibration control. *IEEE Transactions on Control Systems Technology*, *6*(1), 111–120.

Karnopp, D. (1966). Coupled vibratory-system analysis, using the dual formulation. *The Journal of the Acoustical Society of America*, *40*(2), 380–384.

Karnopp, D., Margolis, D. L., & Rosenberg, R. C. (2000). *System dynamics: Modeling and simulation of mechatronic systems* (3rd ed.). New York, NY: Horizon Publishers and Distributors Inc.

Karnopp, D. C., Margolis, D. L., & Rosenberg, R. C. (2012). *System dynamics: Modeling, simulation, and control of mechatronic systems* (5th ed.). John Wiley & Sons.

Krenk, S., & Hogsberg, J. (2009). Optimal resonant control of flexible structures. *Journal of Sound and Vibration*. *323* (3–5), 530–554.

Lozano, R., Brogliato, B., Egelund, O., & Maschke, B. (2000). *Dissipative systems: Analysis and control*. New York, NY: Springer.

Margolis, D. L. (1985). A survey of bond graph modelling for interacting lumped and distributed systems. *Journal of the Franklin Institute*, *319*, 125–135.

Marquis-Favre, W., & Jardin, A. (2011). Bond graphs and inverse modeling for mechatronic system design. In W. Borutzky (Ed.), *Bond graph modelling of engineering systems* (pp. 195–226). New York, NY: Springer.

Moheimani, S. O. R, & Behrens, S. (2004). Multimode piezoelectric shunt damping with a highly resonant impedance. *IEEE Transactions on Control Systems Technology*, *12*(3), 484–491.

Moheimani, S. O. R., & Fleming, A. J. (2006). *Piezoelectric transducers for vibration control and damping*. Advances in Industrial Control. New York, NY: Springer.
Mukherjee, A., Karmaker, R., & Samantaray, A. K. (2006). *Bond graph in modeling, simulation and fault indentification*. New Delhi: I.K. International.
Ortega, R., Loria, A., Nicklasson, P. J., & Sira-Ramirez, H. (1998). *Passivity-based control of Euler-lagrange systems*. London: Springer.
Ortega, R., Praly, L., & Landau, I. D. (1985). Robustness of discrete-time direct adaptive controllers. *IEEE Transactions on Automatic Control*, *AC-30*(12), 1179–1187.
Ortega, R., van der Schaft, A. J., Mareels, I., & Maschke, B. (2001). Putting energy back in control. *IEEE Control Systems Magazine*, *21*(2), 18–33.
Pintelon, R., & Schoukens, J. (2001). *System identification. A frequency domain approach*. New York, NY: IEEE Press.
Preumont, A. (2002). Vibration control of active structures: An introduction, volume 96 of *Solid mechanics and its applications*. Dordrecht: Kluwer.
Samanta, B., & Mukherjee, A. (1985). A bond graph based analysis of coupled vibratory systems taking advantage of the dual formulation. *Journal of the Franklin Institute*, *320*, 111–131.
Samanta, B., & Mukherjee, A. (1990). Analysis of acoustoelastic systems using modal bond graphs. *Journal of Dynamic Systems, Measurement, and Control*, *112*(1), 108–115.
Sharon, A., Hogan, N., & Hardt, D. E. (1991). Controller design in the physical domain. *Journal of the Franklin Institute*, *328*(5–6), 697–721.
Shearer, J. L., Murphy, A. T., & Richardson, H. H. (1971). *Introduction to system dynamics*. Reading, MA: Addison-Wesley.
Slotine, J. E., & Li, W. (1991). *Applied nonlinear control*. Englewood Cliffs: Prentice-Hall.
Vink, D., Ballance, D., & Gawthrop, P. (2006). Bond graphs in model matching control. *Mathematical and Computer Modelling of Dynamical Systems*, *12*(2–3), 249–261.
Wagg, D., Neild, S., & Gawthrop, P. (2008). Real-time testing with dynamic substructuring. In O. S. Bursi and D. Wagg (Eds.), *Modern testing techniques for structural systems*, volume 502 of *CISM courses and lectures*, Chapter 7 (pp. 293–342). Wien, NY: Springer.
Willems, J. C. (1972). Dissipative dynamical systems, part I: General theory, part II: Linear system with quadratic supply rates. *Arch. Rational Mechanics and Analysis*, *45*(5), 321–351.

Appendix. Derivation of Equation (14)

Equation (14) can be derived directly from the bond graph of Figure 4(a). Letting F and v be the force and velocity at the component interface, letting F_{mr} be the force acting on the mass and damper and F_c the spring force, it follows that the components represented by **I**:**m**, **C**:**k** and **R**:**r** have equations:

$$m\frac{\mathrm{d}v_m}{\mathrm{d}t} = F_{mr}, \tag{A1}$$

$$\frac{\mathrm{d}F_c}{\mathrm{d}t} = kv, \tag{A2}$$

$$v_r = \frac{1}{r}F_{mr}. \tag{A3}$$

Taking Laplace transforms (with zero initial conditions) it follows that:

$$\begin{aligned} v &= v_r + v_m \\ &= \left[\frac{1}{r} + \frac{1}{ms}\right] F_{mr} \\ &= \left[\frac{1}{r} + \frac{1}{ms}\right] (F - F_c) \\ &= \left[\frac{1}{r} + \frac{1}{ms}\right] \left[F - \frac{k}{s}v\right] \\ &= \frac{ms + r}{mrs}\left[F - \frac{k}{s}v\right]. \end{aligned} \tag{A4}$$

Collecting terms in Equation (A4) gives:

$$\frac{k(ms + r) + mrs^2}{s(ms + r)}v = F. \tag{A5}$$

Hence, rearranging Equation (A5):

$$\frac{v}{F} = \frac{s(ms + r)}{mrs^2 + kms + kr}. \tag{A6}$$

The right-hand side of Equation (A6) corresponds to the transfer function of Equation (14).